

# Nonlinear coherent dynamics of an atom in an optical lattice

V.Yu. Argonov and S.V. Prants

Laboratory of Nonlinear Dynamical Systems,  
V.I.Il'ichev Pacific Oceanological Institute  
of the Russian Academy of Sciences, 43 Baltiiskaya st.,  
690041 Vladivostok, Russia

August 8, 2018

## Abstract

We consider a simple model of lossless interaction between a two-level single atom and a standing-wave single-mode laser field which creates a one-dimensional optical lattice. Internal dynamics of the atom is governed by the laser field which is treated to be classical with a large number of photons. Center-of-mass classical atomic motion is governed by the optical potential and the internal atomic degree of freedom. The resulting Hamilton-Schrödinger equations of motion are a five-dimensional nonlinear dynamical system with two integrals of motion, the total atomic energy and the length of the Bloch vector are conserved during the interaction. In our previous papers the motion of the atom has been shown to be regular or chaotic (in the sense of exponential sensitivity to small variations in initial conditions and/or the system's control parameters) in dependence on values of the control parameters, the atom-field detuning and recoil frequency. At exact atom-field resonance, exact solutions for both the external and internal atomic degrees of freedom can be derived. The center-of-mass motion does not depend in this case on the internal variables, whereas the Rabi oscillations of the atomic inversion is a frequency modulated signal with the frequency to be defined by the atomic position in the optical lattice. We study analytically correlations between the Rabi oscillations and the center-of-mass motion in two limiting cases of a regular motion out off the resonance: (1) far-detuned atoms and (2) fastly moving atoms. The main focus of the paper is chaotic atomic motion that may be quantified strictly by positive values of the maximal Lyapunov exponent. It is shown that atom, depending on the value of its total energy, can either oscillate chaotically in a well of the optical potential or fly ballistically with weak chaotic oscillations of its momentum or wander in the optical lattice changing the direction of motion in a chaotic way. In the regime of chaotic wandering atomic motion is shown to have fractal properties. We find a useful tool to visualize complicated atomic motion — Poincaré mapping of atomic trajectories in an effective three-dimensional phase space onto planes of atomic internal variables and momentum. The Poincaré mappings are constructing using a translational invariance of the standing laser wave. We find common features with typical non-hyperbolic Hamiltonian systems — chains of resonant islands of different sizes imbedded in a stochastic sea, stochastic layers, bifurcations, and so on. The phenomenon of sticking of atomic trajectories to boundaries of regular islands, that should

have a great influence to atomic transport in optical lattices, is found and demonstrated numerically.

PACS 42.50.Vk, 05.45.Mt, 05.45.Xt

## 1 Introduction

Light exerts mechanical forces on matter. This hypothesis was suggested by Kepler [1] in 1619 to explain a deviation of the comet's tails flying nearby the Sun. It was Maxwell who in 1873 estimated the light pressure, using his theory of electromagnetism [2], and has shown that it is very small. Peter Lebedev was the first who in 1899 measured the light pressure on a macroscopic body [3]. The first experiments on deviation of microscopic particles by light have been carried out by W. Gerlach and O. Stern [4], by P. Kapitza and P. Dirac [5], and by O. Frisch [6].

Manipulation of atomic motion with the help of laser beams, creating an optical lattice, is one of the most fastly growing field of modern physics (for a review see, for example, [7]). There are different theoretical and experimental aspects of this interaction including cooling and trapping of atoms, Bose-Einstein condensation, quantum computing and processing information with atoms.

In this paper we review our recent results on nonlinear coherent dynamics of a single two-level atom in an optical lattice created in a one-dimensional cavity by two counterpropagating laser waves. We are working in the strong-coupling regime and neglect all the losses. We show that even in a one-dimensional approximation the atomic motion can be very complicated. We analyze both regular and chaotic motion of atoms in a stationary standing-wave laser field containing a large number of photons. It should be stressed that there is a difference between various types of erratic atomic motion in an optical lattice. *Chaotic motion* is strictly defined as a motion of a deterministic nonlinear dynamical system that is exponentially sensitive to small variations in the system's initial conditions or/and its control parameters. There are different types of chaotic motion of atoms in an optical lattice, including chaotic nonlinear oscillations of atomic center of mass in a well of the optical potential, chaotic ballistic motion, when the atomic momentum oscillates chaotically around a value of the average momentum, and the last but not least, *chaotic wandering* of an atom when it changes its direction of motion in a chaotic way [8, 9, 10, 11, 12, 13]. All the types of chaotic atomic motion are quantified by positive values of the maximal Lyapunov exponent.

In an optical lattice chaotic motion in the strict sense of this notation may occur when there is no any kind of noise, including atomic spontaneous emission which is a random process. The respective deterministic atomic equations of motion are approximate ones, but they are fundamental since spontaneous emission may be considered as a quantum noise. *Random walking* is a kind of motion that occurs with ultracold atoms which are detuned far away from the carrier laser frequency, so their internal degrees of freedom can be eliminated adiabatically. Because the values of the momentum of ultracold atoms are compared with the value of the photon momentum, each time after emitting a spontaneous photon atom gets a kick in a random direction. This effect is a quantum analogue of the classical random walking.

In a general situation we should take into account both the internal atomic motion and spontaneous emission events. In this case, however, the equations of motion cease to be a deterministic dynamical system because they include random terms and one may expect much more complicated type of atomic motion which, besides of chaotic motion, caused by the fun-

damental atom-field interaction, includes a purely stochastic component caused by random events of spontaneous emission. We have shown recently that in a range of the control parameters (detuning, laser intensity, and recoil frequency) and initial conditions atoms may change their direction of motion erratically even if their momenta are much larger than the photon momentum. We will call this type of motion as *chaotic walking*.

The main aim of this paper is to describe different aspects of deterministic atomic motion in an optical lattice, both regular and chaotic ones. The effects of spontaneous emission on the atomic motion will be considered in a forthcoming paper.

## 2 Hamilton-Schrödinger equations of motion

We consider a two-level atom with mass  $m_a$  and transition frequency  $\omega_a$ , moving with the momentum  $P$  along the axis  $X$  in an ideal cavity through the standing laser wave with the field frequency  $\omega_f$  and the wave vector  $k_f$ . In the frame, rotating with the frequency  $\omega_f$ , the standard cavity QED Hamiltonian is the following:

$$\hat{H} = \frac{\hat{P}^2}{2m_a} + \frac{1}{2}\hbar(\omega_a - \omega_f)\hat{\sigma}_z - \hbar\Omega(\hat{\sigma}_- + \hat{\sigma}_+)\cos k_f\hat{X}. \quad (1)$$

Here  $\hat{\sigma}_{\pm,z}$  are the Pauli operators which describe the transitions between lower,  $|1\rangle$ , and upper,  $|2\rangle$ , states.  $\Omega$  is the Rabi frequency which is proportional to the square root of the number of photons in the wave  $\sqrt{n}$ . The standing-wave field must be strong enough ( $n \gg 1$ ), so we can neglect a back reaction of atoms on it and consider the field classically. For electronic degree of freedom the simple wavefunction is

$$|\Psi(t)\rangle = a(t)|2\rangle + b(t)|1\rangle, \quad (2)$$

where  $a$  and  $b$  are the complex-valued probability amplitudes to find the atom in the states  $|2\rangle$  and  $|1\rangle$ , respectively. Using the Hamiltonian (1), we get the Schrödinger equation

$$\begin{aligned} i\frac{da}{dt} &= \frac{\omega_a - \omega_f}{2}a - \Omega b \cos k_f X, \\ i\frac{db}{dt} &= \frac{\omega_f - \omega_a}{2}b - \Omega a \cos k_f X, \end{aligned} \quad (3)$$

where the atomic position  $X$  is considered as a parameter. Let us introduce instead of the complex-valued probability amplitudes  $a$  and  $b$  the following new real-valued variables:

$$u \equiv 2\operatorname{Re}(ab^*), \quad v \equiv -2\operatorname{Im}(ab^*), \quad z \equiv |a|^2 - |b|^2, \quad (4)$$

which are the quadratures of the atomic dipole moment ( $u$  and  $v$ ) and the atomic population inversion,  $z$ .

In the process of emitting and absorbing photons, atoms not only change their internal electronic states but their external translational states change as well due to the photon recoil. If the atomic average momentum is large as compared to the photon momentum  $\hbar k_f$ , one can describe the translational degree of freedom classically satisfying to classical Hamilton

equations of motion. The dynamics in the strong-coupling regime is now governed by the Hamilton-Schrödinger equations

$$\begin{aligned}
\dot{x} &= \omega_r p, \\
\dot{p} &= -u \sin x, \\
\dot{u} &= \Delta v, \\
\dot{v} &= -\Delta u + 2z \cos x, \\
\dot{z} &= -2v \cos x,
\end{aligned} \tag{5}$$

where  $x \equiv k_f \langle \hat{X} \rangle$  and  $p \equiv \langle \hat{P} \rangle / \hbar k_f$  are classical atomic center-of-mass position and momentum, respectively. Dot denotes differentiation with respect to dimensionless time  $\tau \equiv \Omega t$ . The normalized recoil frequency,  $\omega_r \equiv \hbar k_f^2 / m_a \Omega \ll 1$ , and the atom-field detuning,  $\Delta \equiv (\omega_f - \omega_a) / \Omega$ , are the control parameters. The system has two integrals of motion, namely the total energy

$$W \equiv \frac{\omega_r}{2} p^2 + U, \tag{6}$$

where

$$U \equiv -u \cos x - \frac{\Delta}{2} z, \tag{7}$$

is the potential energy, and the Bloch vector

$$u^2 + v^2 + z^2 = 1. \tag{8}$$

The conservation of the Bloch vector length immediately follows from Eqs. (4).

Equations (5) with two integrals of motion constitute a Hamiltonian autonomous system with two degrees of freedom and motion on a three-dimensional hypersurface with a given energy value  $W$ . Generally, such a system has a positive Lyapunov exponent  $\lambda$ , a negative exponent equal in magnitude to positive one, and two zero exponents. The sum of all Lyapunov exponents of a Hamiltonian system is zero [14]. The maximal Lyapunov exponent characterizes the mean rate of the exponential divergence of initially close trajectories,

$$\lambda = \lim_{\tau \rightarrow \infty} \lambda(\tau), \quad \lambda(\tau) = \lim_{\delta(0) \rightarrow 0} \frac{1}{\tau} \ln \frac{\delta(\tau)}{\delta(0)}, \tag{9}$$

and serves as a quantitative measure of dynamical chaos in the system. Here,  $\delta(\tau)$  is a distance (in the Euclidian sense) at time  $\tau$  between two trajectories close to each other at initial time  $\tau = 0$ . The dependence of  $\lambda$  on control parameters has been calculated in [8, 9] with the similar system. It has been shown that dynamical chaos in a strongly-coupled atom-field system exist in a wide range of parameters and initial atomic momentum  $p_0$ . The result of computation of the maximal Lyapunov exponent with our system (5) in the space of control parameters,  $\omega_r$  and  $\Delta$ , is shown in Fig. 1. In white regions of the map maximal Lyapunov exponent  $\lambda$  is almost zero and the dynamics is stable. In other regions the positive values of  $\lambda$  show the Lyapunov instability.

In all the numerical simulations we use physically realistic parameters and initial conditions. For example, we can chose cesium atoms with the transition wavelength  $\lambda_a \simeq 852$  nm. The Rabi frequency  $\Omega$  depends on many factors including the field strength, which could be changed in a wide range. In most computations we shall use the Rabi frequency of  $\Omega \approx 10$  GHz. With this value of the Rabi frequency we get the normalized recoil frequency to be  $\omega_r = 10^{-5}$ . Also

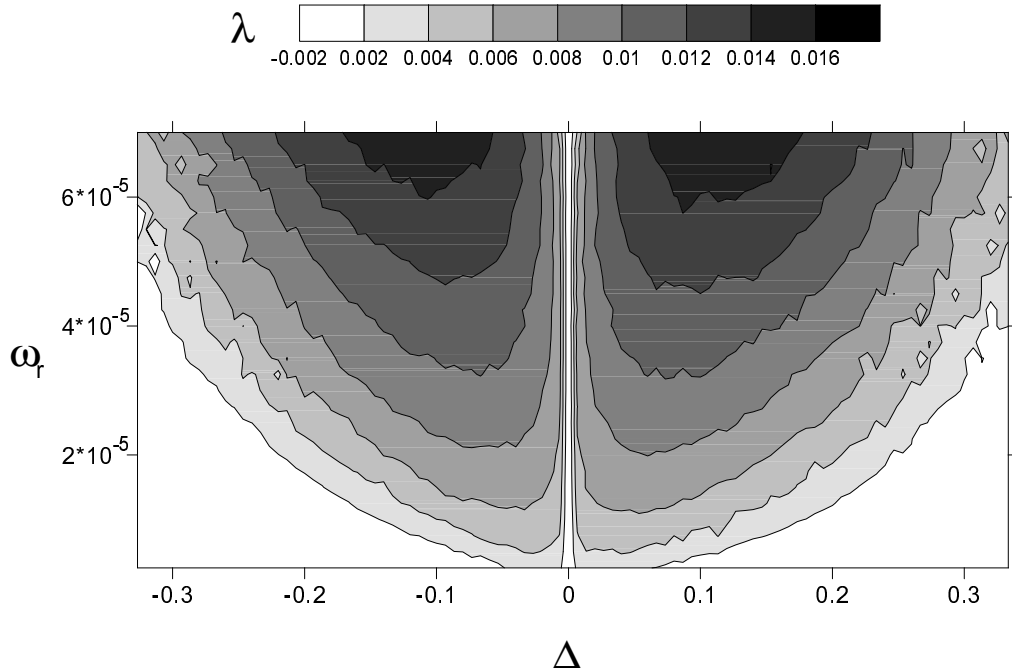


Figure 1: Maximal Lyapunov exponent  $\lambda$  vs the detuning  $\Delta$  and the normalized recoil frequency  $\omega_r$ :  $p_0 = 200$ ,  $z_0 = -1$ ,  $u_0 = v_0 = 0$ .

we put the initial position  $x_0 = 0$ . The detuning  $\Delta$  could be varied in a wide range, and the Bloch variables are restricted by the length of the Bloch vector (8). The most interesting effects are observed with rather cold atoms. For example,  $p_0 = 200$  taken in computing  $\lambda$  in Fig. 1 with our normalization corresponds to the atomic velocity  $v_a \approx 0.7$  m/s. It should be noted that we use in this paper the normalization to the laser Rabi frequency  $\Omega$ , not to the vacuum (or single-photon) Rabi frequency as it has been done in our previous papers [8, 9, 10, 11, 12]. So the ranges of the normalized control parameters, taken in this paper, differ from those in the cited papers.

### 3 Regular dynamical regime

#### 3.1 Exact atom-field resonance

At exact resonance,  $\Delta = 0$ , one can easily find an additional integral of motion,

$$u = \text{const} = u_0. \quad (10)$$

In this case the fast and slow variables are separated from each other allowing one to integrate exactly the reduced equations of motion. Total energy becomes equal to

$$W_R = \frac{\omega_r}{2} p^2 - u_0 \cos x, \quad (11)$$

and the potential energy gets the simple form

$$U_R = -u_0 \cos x. \quad (12)$$

The center-of-mass translational motion of the atom in such a spatially periodic potential of the standing wave is described by the simple nonlinear equation for a free physical pendulum

$$\ddot{x} + \omega_r u_0 \sin x = 0, \quad (13)$$

and does not depend on evolution of the internal degrees of freedom.

The translational motion is trivial when  $u_0$  is zero. In spite of the zero potential field, a structure of a standing wave is still present in a cavity. In this case, the atom will move in one direction with a constant velocity, and the Rabi oscillations modulated by the standing wave will occur. In general case one can easily get from (11) the dependence  $p(x)$

$$p = \sqrt{\frac{2}{\omega_r}(W_R + u_0 \cos x)}, \quad (14)$$

which gives the phase portrait of the system in the plane  $(x, p)$  (Fig. 2a). It is the phase portrait of a nonlinear pendulum with three types of trajectories depending on the value of its energy  $W_R$ : oscillator-like motion in a potential well if  $W_R < u_0$ , a separatrix if  $W_R = u_0$ , and ballistic-like motion if  $W_R > u_0$ .

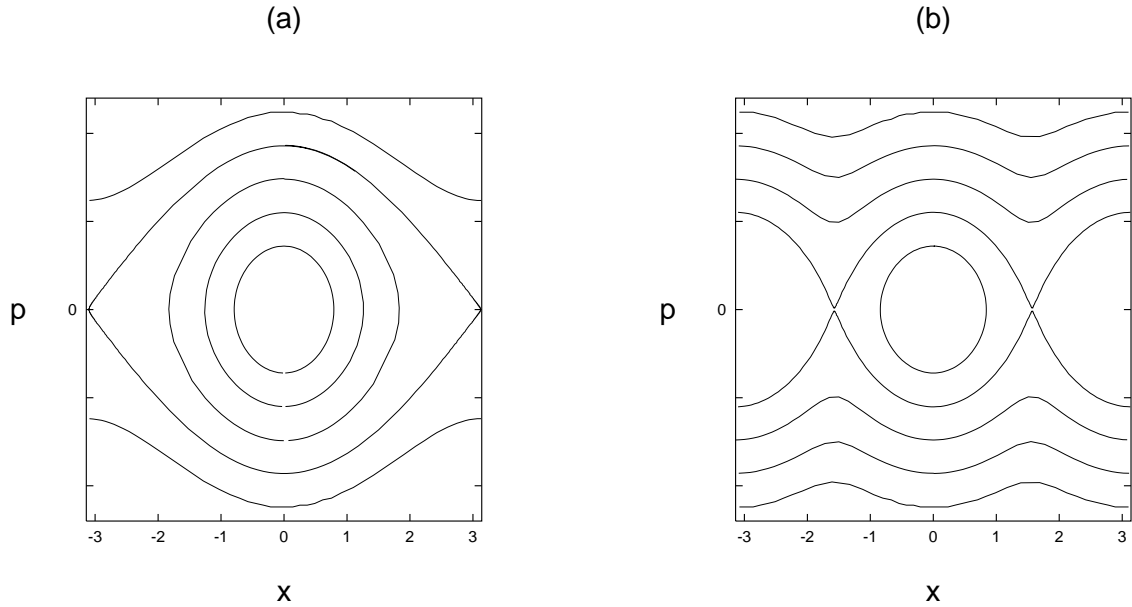


Figure 2: The typical regular phase portraits for the translational degree of freedom: (a)  $\Delta = 0$ ; (b)  $|\Delta| \gtrsim 0.2$ .

For the initial values  $x_0 = 0$  and  $\dot{x}_0 = \omega_r p_0$ , the equation for the translational motion (13) has the solution

$$x(\tau) = \begin{cases} 2 \arcsin [K \operatorname{sn} [\sqrt{\omega_r u_0} \tau, K]], & K^2 \leq 1; \\ 2 \operatorname{am} \left[ \frac{1}{2} \omega_r p_0 \tau, \frac{1}{K} \right], & K^2 \geq 1, \end{cases} \quad (15)$$

$$p(\tau) = \begin{cases} p_0 \operatorname{cn} [\sqrt{\omega_r u_0} \tau, K], & K^2 \leq 1; \\ p_0 \operatorname{dn} \left[ \frac{1}{2} \omega_r p_0 \tau, \frac{1}{K} \right], & K^2 \geq 1, \end{cases} \quad (16)$$

where

$$K = \frac{p_0}{2} \sqrt{\frac{\omega_r}{u_0}} \quad (17)$$

is the modulus of the elliptic Jacobi functions. The solution gives the critical value of the atomic momentum

$$p_{cr} = 2\sqrt{u_0/\omega_r}. \quad (18)$$

Atoms with  $p_0 \leq p_{cr}$  are trapped by the standing-wave field, the result that is well-known from early studies [15]. The modulus  $K$  is simply connected with the normalized value of the difference between the energy of the atom and its value on the separatrix

$$K^2 = 1 + \frac{W_R - u_0}{2u_0}. \quad (19)$$

As to internal atomic evolution, it depends on the translational degree of freedom since the force of the atom-field coupling depends on the position of the atom in a periodic standing-wave potential. The equation for the atomic population inversion  $z(\tau)$  is derived from the two last equations of the set (5) with  $\Delta = 0$ :

$$\dot{z} = \mp 2\sqrt{1 - z^2 - u_0^2} \cos[x(\tau)], \quad (20)$$

where  $\cos[x(\tau)]$  is a known function of the translational variables only which can be found with the help of the exact solutions obtained. It is easy to find the exact solution of Eq. (20)

$$z(\tau) = \mp \sqrt{1 - u_0^2} \sin\left(2 \int_0^\tau \cos x d\tau' + \psi_0\right), \quad (21)$$

where the sign is opposite to that for the initial value  $z_0$  and

$$\psi_0 = \mp \arcsin \frac{z_0}{\sqrt{1 - u_0^2}} \quad (22)$$

is an integration constant. The internal energy of the atom could be considered as a frequency-modulated signal with the instant frequency  $2 \cos[x(\tau)]$  and the modulation frequency  $\dot{x} = \omega_r p(\tau)$ , but it is correct only if the first value is much greater than the second, i. e.  $|\omega_r p_0| \ll 2$ . Such a signal is shown in Fig. 3a for a ballistic atom ( $p_0 = 5000$ ,  $v_a \approx 17.5$  m/s). With  $|\omega_r p_0| \geq 2$  the modulation disappears and the signal becomes a periodic one with the frequency  $\omega_r p$ . With fast atoms,  $|\omega_r p_0| \gg 2$  and  $p \simeq p_0 \gg p_{cr}$  (Raman-Nath approximation) Eq. (21) is simplified

$$z(\tau) \approx z_0 - \frac{2v_0}{\omega_r p_0} \sin \omega_r p_0 \tau - \frac{4z_0}{\omega_r^2 p_0^2} \sin^2 \omega_r p_0 \tau. \quad (23)$$

### 3.2 Non-resonant Rabi oscillations

With comparatively small detunings  $\Delta$  the dynamics of slow atoms can be chaotic. In this case the Rabi oscillations are still a signal with a frequency modulation, but the amplitude is not constant anymore, it jumps chaotically with the characteristic time  $1/\omega_r p$ . With comparatively large detunings, the Rabi oscillations become regular, but with a prominent periodic amplitude modulation, while the frequency modulation is not so deep (Fig. 3b).

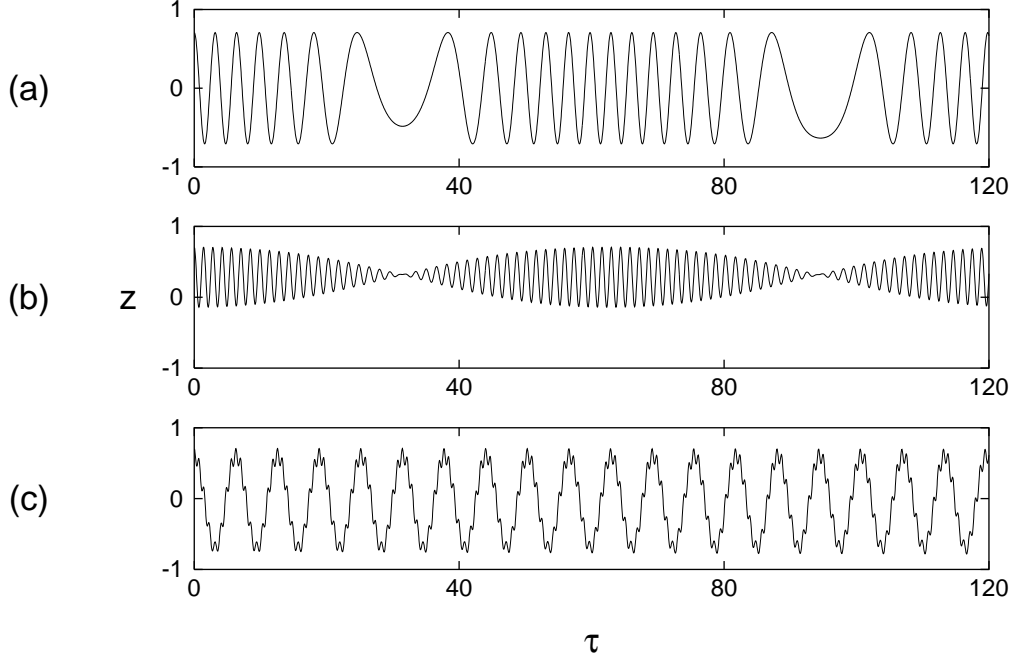


Figure 3: Rabi oscillations: (a) frequency modulation at exact resonance,  $\Delta = 0$ ,  $p_0 = 5000$ ; (b) amplitude modulation far from resonance,  $\Delta = -4$ ,  $p_0 = 5000$ ; (c) Doppler-Rabi resonance,  $\Delta = -4$ ,  $p_0 = 400000$ . In all panels,  $z_0 = u_0 = \sqrt{0.5}$ ,  $v_0 = 0$ .

In two limit cases,  $|\Delta| \gg \max[|\omega_r p|, 2]$  and  $|\omega_r p| \gg \max[|\Delta|, 2]$ , the analytic solutions can be obtained. In this both cases  $u$  and  $v$  are the harmonic functions with the frequency  $\Delta$ , and for the internal energy we have

$$z \approx \begin{cases} z_0 + \frac{2u_0}{\Delta} - \frac{2\sqrt{u_0^2 + v_0^2}}{\Delta} \cos x \sin(\Delta\tau + \varphi_0), & |\Delta| \gg \max[|\omega_r p|, 2], \\ z_0 + \frac{2\sqrt{u_0^2 + v_0^2}}{\omega_r p_0} \cos(\Delta\tau + \varphi_0) \sin \omega_r p_0 \tau, & |\omega_r p_0| \gg \max[|\Delta|, 2], \omega_r p_0^2 \gg 4, \end{cases} \quad (24)$$

where  $\varphi_0 = \arcsin(u_0/\sqrt{u_0^2 + v_0^2})$ . The Rabi oscillations now are amplitude-modulated signals with two characteristic frequencies  $|\omega_r p|$  and  $|\Delta|$ . The larger frequency is the main frequency and the other one is the modulation frequency. In the solution for fast atoms we also used the Raman-Nath approximation,  $x \simeq \omega_r p_0 \tau$ , that is correct if the initial kinetic energy  $\omega_r p_0^2/2$  is much greater than the amplitude of potential energy variations (equal to 2 in our case). With  $\Delta = 0$ , the solution has the form (23), but without the last term which is small. Solutions (24) show a good correspondence with the numerical experiments, performed in [12] with the similar equations. The typical amplitude-modulated Rabi oscillations are shown in Fig. 3b.

More exact solution for  $u$  can be found using the approximation  $z \approx \text{const} \approx z_0$  (i. e.  $z_{\max} - z_{\min} \ll |z_0|$ ), which is correct in the both limit cases considered above, excluding  $z_0 \approx 0$ . Then from Eq. (5) we get the equation for a driven linear oscillator

$$\ddot{u} + \Delta^2 u \approx 2z_0 \Delta \cos x, \quad (25)$$



which has the solution

$$u(\tau) \approx 2z_0 \sin \Delta \tau \int \cos \Delta \tau \cos x d\tau - 2z_0 \cos \Delta \tau \int \sin \Delta \tau \cos x d\tau + u_0 \cos \Delta \tau + v_0 \sin \Delta \tau. \quad (26)$$

For  $|\Delta| \gg |\omega_r p|$ , the solution (26) can be approximated as follows:

$$u \approx \frac{2z_0}{\Delta} \cos x + \sqrt{u_0^2 + v_0^2} \sin(\Delta \tau + \varphi_0). \quad (27)$$

Using Eqs. (24) and (27), we get the periodic potential with the spatial period  $\pi$  (in difference from the resonant potential with the period  $2\pi$ ):

$$U \approx -\frac{2z_0}{\Delta} \cos^2 x + \text{const.} \quad (28)$$

The corresponding phase portrait is shown in Fig. 2b.

When the frequencies are close,  $|\omega_r p| \simeq |\Delta|$ , the Doppler-Rabi resonance takes place [12] in spite of the fact that the detuning may be very large. Let us consider the standing wave as a combination of two counter-propagating waves. In the frame, moving with the atomic velocity, their frequencies,  $\omega_1$  and  $\omega_2$ , are different because of the Doppler effect:

$$\omega_1 = \omega_f - \frac{v_a}{c} \omega_f, \quad \omega_2 = \omega_f + \frac{v_a}{c} \omega_f, \quad (29)$$

where  $v_a$  is the atomic velocity and  $c$  is the speed of light. The atom is rather slow so we can neglect the relativistic effects. Let us consider atoms fast enough for the Raman-Nath approximation  $p \approx p_0$  to be valid. Renormalizing all the frequencies to  $\Omega$ , we define the dimensionless detunings between the atomic transition and the running wave frequencies as:

$$\Delta_1 \equiv \frac{\omega_1 - \omega_a}{\Omega} = \Delta - \omega_r p_0, \quad \Delta_2 \equiv \frac{\omega_2 - \omega_a}{\Omega} = \Delta + \omega_r p_0. \quad (30)$$

The condition  $|\Delta| = |\omega_r p_0|$  leads to the resonance between the atom and one of the waves. If  $|\Delta| \gg 1$ , we can neglect the interaction with the other wave and consider the atom as if only one wave with the frequency  $\omega_1$  or  $\omega_2$  exists. In the field of the wave, say,  $\omega_1$ , the dynamics can be described by the Bloch-like equations

$$\dot{u} = \Delta_1 v, \quad \dot{v} = -\Delta_1 u + z, \quad \dot{z} = -v, \quad (31)$$

in which the interaction energy does not depend on the atomic position and its amplitude value is twice smaller as compared to the standing wave. Eqs. (31) have the solution

$$z = \frac{u_0 \Delta_1}{\omega_z^2} (1 - \cos \omega_z \tau) - \frac{v_0}{\omega_z} \sin \omega_z \tau + z_0 \left( \frac{\Delta_1^2}{\omega_z^2} + \frac{1}{\omega_z^2} \cos \omega_z \tau \right), \quad (32)$$

where  $\omega_z \equiv \sqrt{\Delta_1^2 + 1} = \sqrt{(\Delta - \omega_r p_0)^2 + 1}$ . At the exact Doppler resonance ( $\Delta_1 = 0$ ), atomic internal energy  $z$  oscillates with the dimensionless frequency 1, and the amplitude of oscillations is maximal. Numerical simulations with Eqs. (5) shows that this speculations are correct (Fig. 2c, where  $p_0 = 400000$  and  $v_a \approx 1400$  m/s), and even very far from the resonance  $\Delta = 0$  the deep Rabi oscillations can be observed for the atoms to be fast enough.

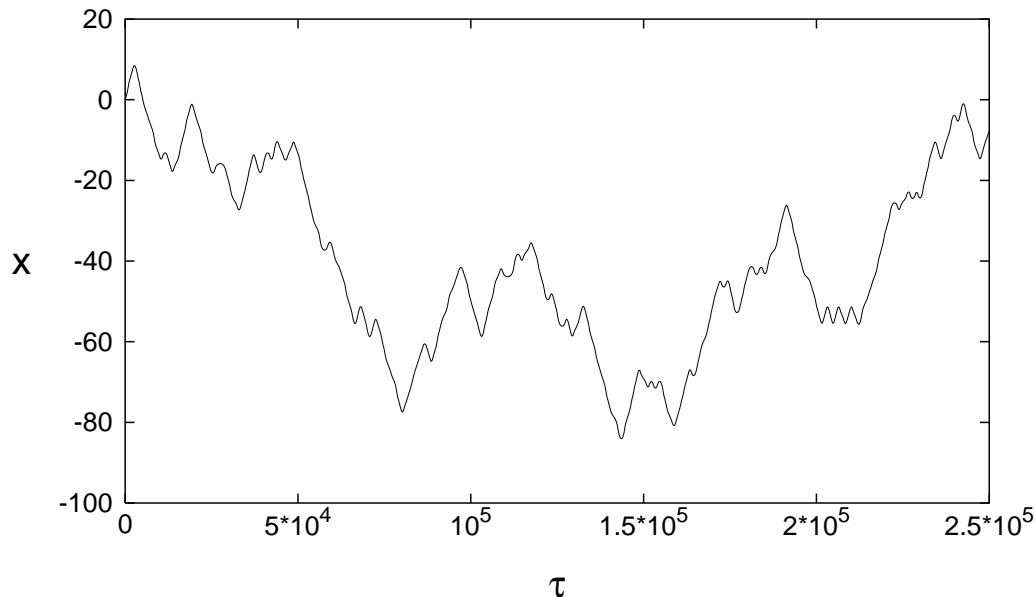


Figure 4: A typical atomic trajectory in the regime of chaotic wandering:  $x_0 = 0$ ,  $p_0 = 300$ ,  $z_0 = -1$ ,  $u_0 = v_0 = 0$ ,  $\omega_r = 10^{-5}$ ,  $\Delta = -0.05$ .

## 4 Irregular dynamics: chaos and fractals

### 4.1 Chaotic atomic wandering

In Fig. 1 we depict the maximal Lyapunov exponent map in the space of control parameters,  $\omega_r$  and  $\Delta$ . The maximal Lyapunov exponent depends not only on the parameters  $\omega_r$  and  $\Delta$ , but on initial conditions of the system (5), as well. Especially important is a value of the initial momentum,  $p_0$ . The most interesting effects can be observed with rather cold atoms, when the initial atomic kinetic energy is close to the amplitude of the optical potential. In this case we get the chaotic wandering of an atom in the standing wave. A typical chaotic atomic trajectory is shown in Fig. 4.

It follows from (5) that the translational motion of the atom at  $\Delta \neq 0$  is described by the equation of a nonlinear physical pendulum with a frequency modulation

$$\ddot{x} + \omega_r u(\tau) \sin x = 0, \quad (33)$$

in which  $u$  is the function of all the other dynamical variables. The normalized Rabi oscillation frequency is a value of the order of  $\omega'_z \equiv \sqrt{\Delta^2 + 4}$  which substantially exceeds the frequency of small-amplitude translational motion  $\sqrt{\omega_r u_0} \ll 1$  in the potential well. Taking this into consideration, the mechanism of the arising of chaos can be revealed [10]. The stochastic layer width was estimated as

$$D \simeq 8\pi \left( \frac{\omega'_z}{\omega_0} \right)^3 \exp \left( \frac{-\pi \omega'_z}{2\omega_0} \right), \quad (34)$$

where  $\omega_0 \equiv \sqrt{2\omega_r |\Delta|} / \omega'_z$ ,  $\omega'_z / \omega_0 \gg 1$ . The  $D$  value is the energy change in the neighbourhood of the unperturbed separatrix normalized with respect to the pendulum separatrix energy  $\omega_0^2$ . Small changes in the energy causes comparatively small changes in the frequency of oscillations.

For the energies of motion that are strongly different from the separatrix energy, that is, close to potential well bottoms and high above optical potential  $U$  hills, small frequency changes cause small phase changes during the translation motion period. However, close to the unperturbed separatrix, where the period of oscillations tends to infinity, even small frequency changes can cause substantial phase changes. This is the reason for the exponential instability of motion of the parametric nonlinear oscillator (33) and chaotic atomic motion in the field of a periodic standing wave.

A clear idea of the character of chaotic wandering can be developed using the model of “two potentials”. At resonance, the optical potential  $U$  reproduces the structure of the standing wave in the cavity (12) with the  $2\pi$  period (the phase portrait in Fig. 2a). Far from the resonance, the potential has the period  $\pi$  and is approximately described by Eq. (28) and the corresponding phase portrait is shown in Fig. 2b. These potentials will be called resonant and nonresonant, respectively. We can say that, when the motion in the cavity is chaotic, the both potentials “virtually” coexist. The well depths in both structures change as time passes, and an atom randomly gets into one or another structure every time when it crosses a standing wave node. The probability of getting into the resonant or nonresonant potentials depends on the detuning. Near the resonance atom is in the resonant potential almost the whole time and only rarely gets into nonresonant one for a short time.

In our study [12] we have shown that chaotic wandering has fractal properties.

## 4.2 Dynamical atomic fractals

In Fig. 5 we depict the scheme of a *gedanken* experiment that consists of a Fabry-Perot optical microcavity with two detectors and cold atoms to be placed in the cavity. To avoid complica-

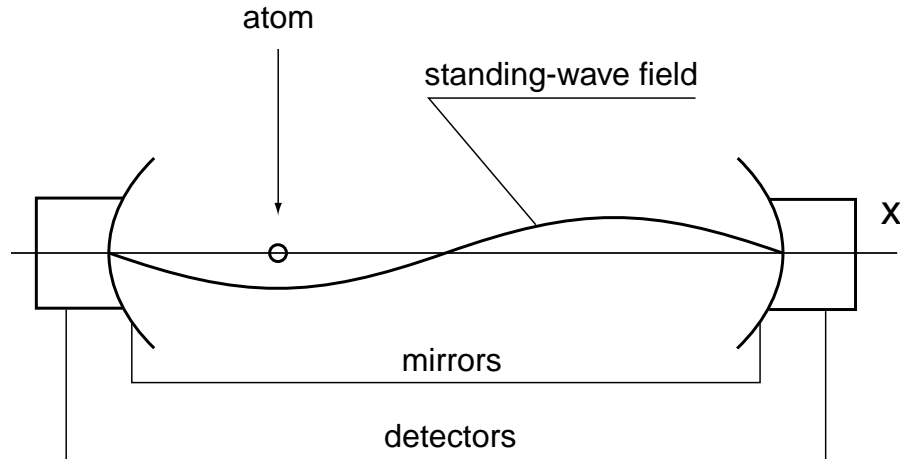


Figure 5: The schematic diagram shows a standing-wave microcavity with detectors.

tions that are not essential to the main theme of this work, we consider the cavity with only two standing-wave lengths. Atoms, one by one, are placed at the point  $x_0 = 0$  with different values of the detuning  $\Delta$ . We measure a time when an atom reaches one of the detectors, the exit time  $T$ , and study the dependence  $T(\Delta)$  under the other equal conditions imposed on the atom and the cavity field. Fig. 6 shows the function  $T(\Delta)$  for atoms with the initial momentum  $p_0 = 200$  ( $v_a \approx 0.7$  m/s). The exit time function demonstrates an intermittency of smooth

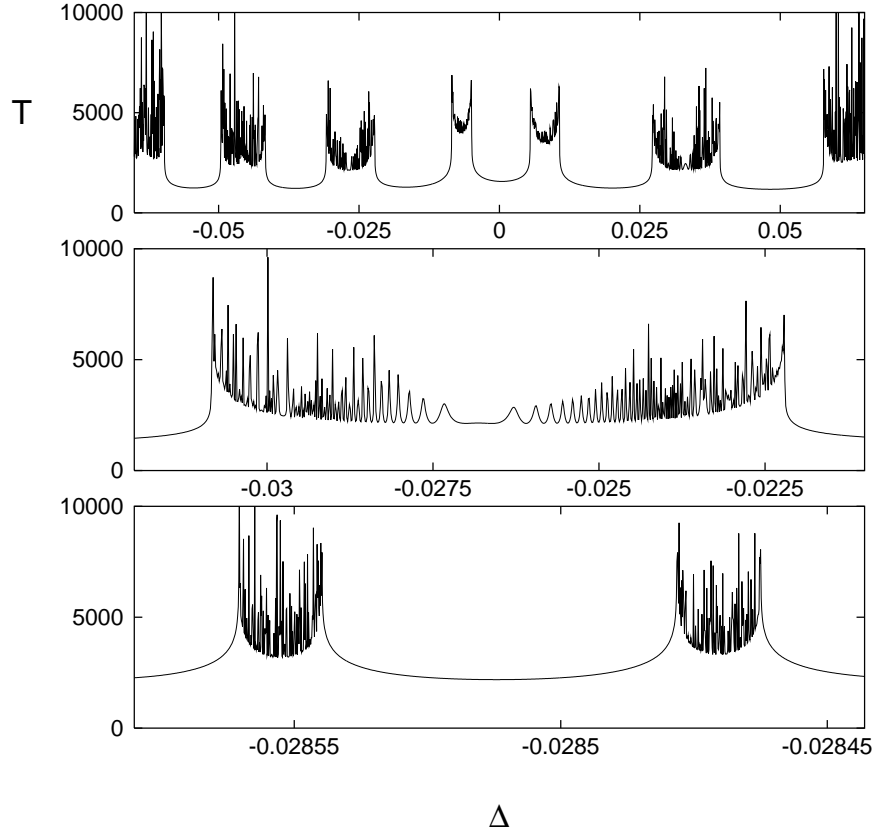


Figure 6: Atomic fractals. Exit time of cold atoms  $T$  vs the detuning  $\Delta$ :  $p_0 = 200$ ,  $z_0 = -1$ ,  $u_0 = v_0 = 0$ .

curves and complicated structures that cannot be resolved in principle, no matter how large the magnification factor. The middle and low panels in Fig. 6 show successive magnifications of the function for the small intervals. Further magnifications reveals a self-similar fractal-like structure that is typical for Hamiltonian systems with chaotic scattering [16].

The exit time  $T$ , corresponding to both smooth and unresolved  $\Delta$  intervals, increases with increasing the magnification factor. Theoretically, there exist atoms never reaching the detectors inspite of the fact that they have no obvious energy restrictions to leave the cavity. Tiny interplay between chaotic external and internal dynamics prevents these atoms from leaving the cavity. The similar phenomenon in chaotic scattering is known as *dynamical trapping*. In [12] for the similar fractal we have computed the Hausdorff dimension and shown that it is not integer.

Different kinds of atomic trajectories before detection can be characterized by the number  $m - 1$  of changing the sign of momentum. An  $m$ -th trajectory corresponds to the atom which changes the direction of motion before being detected  $m - 1$  times. There are also special separatrix-like trajectories following which atoms asymptotically approach to the points with the maximum of potential energy, having no more kinetic energy to overcome it. In difference from the separatrix motion in the resonant system ( $\Delta = 0$ ) with the initial atomic momentum  $p_{cr}$ , a detuned atom can asymptotically reach one of the stationary points even after several oscillations in a well. Let us define the  $mS$ -trajectory as a trajectory when the atom changes the direction of motion  $m - 1$  times and then begin the separatrix-like motion. Such asymptotical motion takes the infinite time, so the atom will never be detected.

The smooth  $\Delta$  intervals in the first-order structure (Fig. 6, upper panel) correspond to atoms which never changes the direction of motion, i. e.  $m = 1$ , and reaching the right detector. The unresolved singular points in the first-order structure with  $T = \infty$  at the border between the smooth and unresolved  $\Delta$  intervals are generated by the  $1S$ -trajectories. Analogously, the smooth and unresolved  $\Delta$  intervals in the second-order structure (Fig. 6, middle panel) correspond to the 2-nd order and the other trajectories, respectively, with singular points between them corresponding to the  $2S$ -trajectories and so on.

There are two different mechanisms of generation of infinite detection times, namely, dynamical trapping with infinite oscillations ( $m = \infty$ ) in a cavity and the separatrix-like motion ( $m \neq \infty$ ). The set of all detunings generating the separatrix-like trajectories is a countable fractal. Each point in the set can be specified as a vector in a Hilbert space with  $m$  integer nonzero components. One is able to prescribe to any unresolved interval of  $m$ -th order structure a set with  $m$  integers, where the first integer is a number of a second-order structure to which trajectory under consideration belongs in the first-order structure, the second integer is a number of a third-order structure in the second-order structure mentioned above, and so on. Such a number set is analogous to a directory tree address: "<a subdirectory of the root directory>/<a subdirectory of the 2-nd level>/<a subdirectory of the 3-rd level>/...". Unlike the separatrix fractal, the set of all detunings leading to dynamically trapped atoms with  $m = \infty$  seems to be uncountable.

The scattering function in the regime of chaotic wandering, time of exit  $T$ , depends in a complicated way not only on the control parameters but initial conditions as well. In Fig. 7 we demonstrate the view of this function, whose values are modulated by color, in two coordinates, the initial atomic momentum  $p_0$  and the atom-field detuning  $\Delta$ . From the fragment (a) to the fragment (f) we increase subsequently the resolution. One can see increasing complexity of the scattering function with a prominent self-similarity. The computation has been performed with the recoil frequency  $\omega_r = 9.17 \cdot 10^{-5}$ .

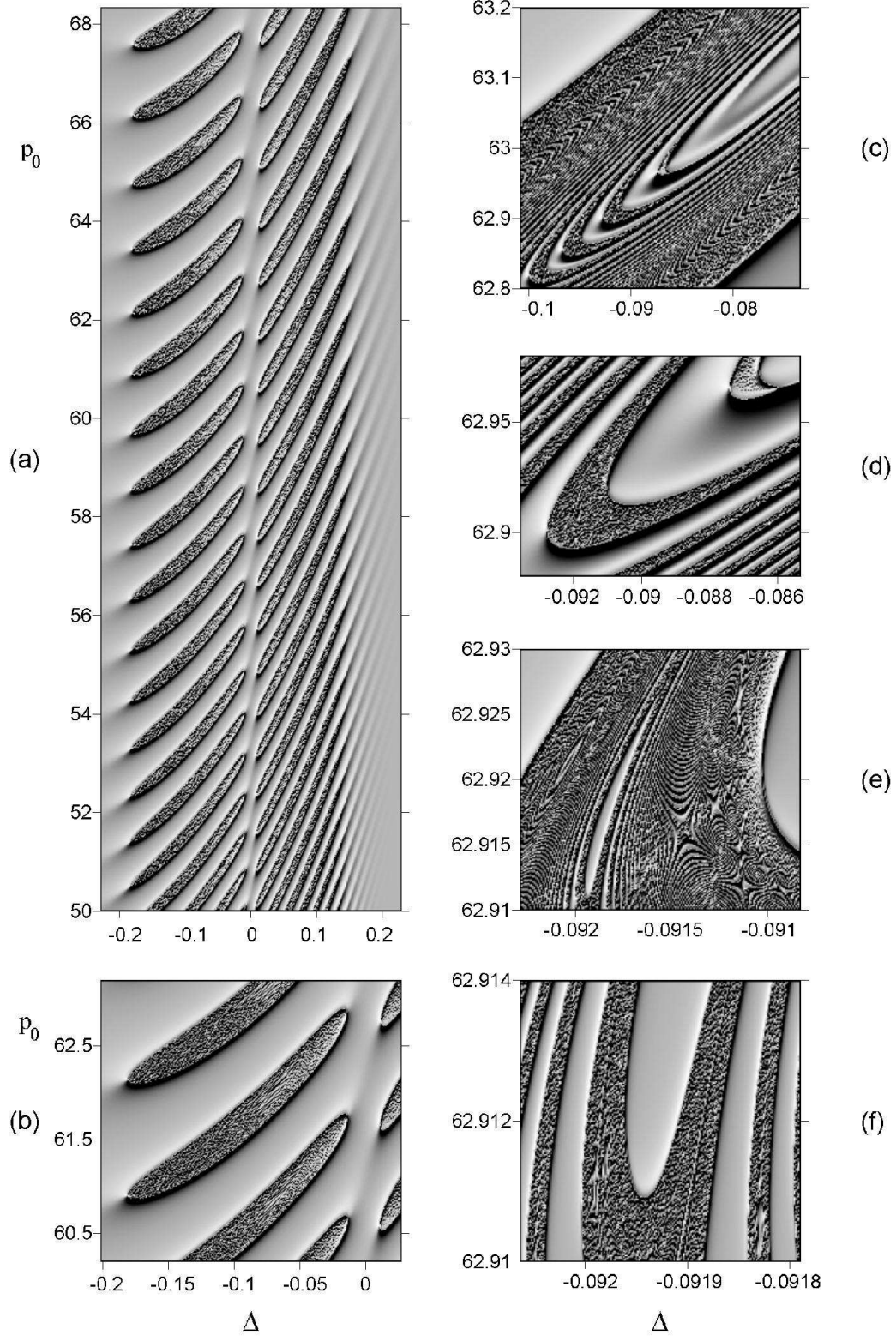


Figure 7: Fractal function of the exit time  $T$  vs the detuning  $\Delta$  and the initial momentum  $p_0$ . The function is shown in a shaded relief regime.  $\omega_r = 9.17 \cdot 10^5$ .



### 4.3 Poincaré mapping

The five variables in the equations of motion (5) minus the two integrals of motion (6) and (8) provide motion in a three-dimensional space. To visualize the motion we use the idea of mapping trajectories on two-dimensional planes. Since we have no time-periodic perturbations in our equations of motion (5) we cannot map trajectories through equal intervals of time provided by a period of a perturbation. However, the system has a characteristic space period  $2\pi$  imposed by the standing wave. So we map trajectories on a chosen plane at those time moments when atoms reach the positions when  $\cos x = 1$ . We close our phase space along the position variable with the period  $2\pi$ . The condition  $\cos x = 1$  under fixed values of the integrals of motion (6) and (8) defines a closed two-dimensional surface in the phase space points of which characterize unambiguously the system's states. In other words, there is a set of points on this two-dimensional surface which corresponds to each trajectory with a given value of the energy  $W$ . This set can be projected onto a plane of any system's variables except for the position  $x$ . Such a projection is, generally speaking, two-valued because the two-dimensional surface is closed. However, one can map trajectories in its "eastern" and "western" parts separately.

In Fig. 8a and b we demonstrate the Poincaré mappings of a number of atomic trajectories in the western ( $u < 0$ ) and eastern ( $u > 0$ ) hemispheres of the Bloch sphere ( $u, v, z$ ) on the plane  $v - z$ , respectively. We fix the values of the detuning  $\Delta = -0.05$ , the recoil frequency  $\omega_r = 10^{-5}$ , the total energy  $W = 33.8$ , the initial position  $x_0 = 0$ , and map the trajectories with different other initial conditions, which are restricted by (6) and (8). All the mappings were obtained with ballistic atoms whose momenta slightly (but chaotically for some initial conditions) oscillate around the effective value  $p_{\text{eff}} = 2600$  that corresponds to the chosen value of the energy. It is such a value of the momentum which an atom has at the moments when its potential energy  $U$  is zero. In Fig. 9 we demonstrate the Poincaré mappings of a number of atomic trajectories in the western ( $u < 0$ ) and eastern ( $u > 0$ ) hemispheres of the Bloch sphere ( $u, v, z$ ) on the plane  $v - z$  just like as in Fig. 8 with  $W = 33.8$  but with another value of the total energy  $W = 36.45$  and the effective momentum  $p_{\text{eff}} = 2700$ . A series of bifurcation occurs just between these values of energy and we get in the end a central critical point instead of a saddle. One can see a typical structure with surviving nonlinear resonances of different orders around the center point and overlapping resonances.

In Figs. 8 and 9 a general views of the mappings in the western and eastern hemispheres are shown. The pictures are rather typical with chaotic Hamiltonian systems [17]. We see regions of regular motion in the form of islands and chains of islands filled by regular trajectories which are known as Kolmogorov-Arnold-Moser (KAM) invariant curves. The islands are imbedded into a stochastic sea, and they are produced by nonlinear resonances of different orders. Increasing the resolution of the mapping, one can see that big islands are surrounded by islands of a smaller size each of which, in turn, is surrounded by a chain of even more smaller islands, and so on to infinity. Stochastic layers of the  $\infty$ -like form are situated between the islands. From the physical point of view, they are formed by broken and overlapping nonlinear resonances. From the mathematical point of view, a stochastic layer is a heteroclinic structure formed by transversal intersections of stable and unstable manifolds of hyperbolic stationary points. A fractal-like structure of generations of islands, a trademark of Hamiltonian chaos, is clearly seen on projections of motion in both the western and eastern hemispheres. To illustrate what happens under increasing the resolution of the Poincaré mapping, we plot in Fig. 8c a zoom of a small region in the stochastic layer in Fig. 8a.

We would like to pay attention to another typical phenomena in Hamiltonian systems, so

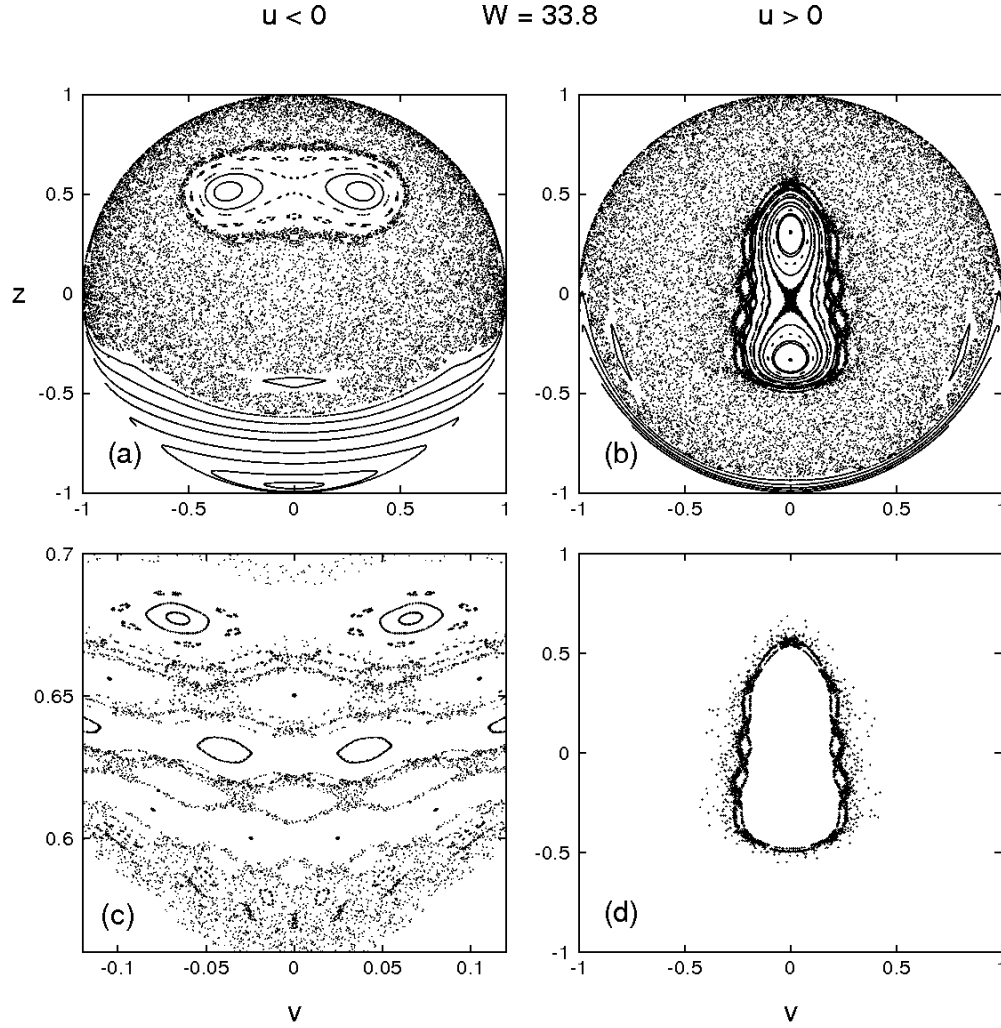


Figure 8: Poincaré mapping in the Bloch variable space. (a)  $u < 0$  (western Bloch hemisphere), (b)  $u > 0$  (eastern Bloch hemisphere), (c) magnification of the small region in (a) fragment, (d) mapping with a single chaotic trajectory in (b) fragment, illustrating the effect of sticking:  $W = 33.8$ ,  $p_{\text{eff}} = 2600$ ,  $\omega_r = 10^{-5}$ ,  $\Delta = -0.05$ .



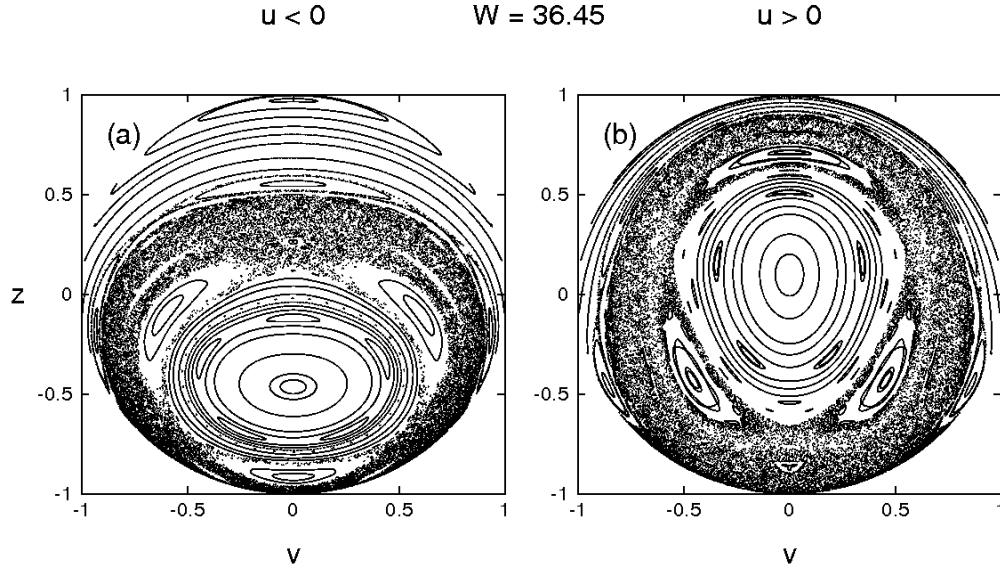


Figure 9: Poincaré mapping in the Bloch variable space. (a)  $u < 0$  (western Bloch hemisphere), (b)  $u > 0$  (eastern Bloch hemisphere). The parameters are the same as in Fig. 8, but  $W = 36.45$ ,  $p_{\text{eff}} = 2700$ .

called sticking [17, 18, 19, 20, 21]. In Fig. 8d we demonstrate the phenomenon of sticking in the eastern Bloch hemisphere. The trajectory shown demonstrates an intermittent type of motion. It wanders for a while in the stochastic sea as a chaotic trajectory, whose instability is characterized by a positive value of the finite-time maximal Lyapunov exponent. Then it is stuck to the boundaries of the outmost visible chain of regular islands, where it is practically regular with zero value of the respective finite-time maximal Lyapunov exponent. It may take a large amount of time to find a gap in a cantori structure, surrounding the outmost KAM tori, and to get off in the stochastic sea. The process is repeated as time grows. It should be stressed that sticking influences strongly transport properties in Hamiltonian systems giving rise to anomalous diffusion, algebraic tails in distributions of the Poincaré recurrence times and of times and lengths of atomic flights.

In Fig. 10a and b we map the same atomic trajectories as in Figs. 8 and 9 onto the plane  $p-z$ . In this case both the parts of the closed two-dimensional surface have the same projections because the set is symmetric with respect to the hyperplane  $v = 0$ .

In order to quantify instability of the trajectories on the Poincaré mappings in Figs. 8 and 9, we have computed the maps of the maximal Lyapunov exponents exactly with the same initial conditions and parameters as in those figures. The results in the  $v_0 - z_0$  coordinates for eastern hemispheres at  $W = 33.8$  and  $W = 36.45$  with  $u > 0$  are shown in Figs. 11a and b, respectively. A rather good correspondence between the Poincaré mapping and the maximal Lyapunov exponents proves that the Poincaré mapping we have constructed is a good means to visualize complicated dynamics of the coupled internal and external atomic degrees of freedom.

The Poincaré mapping with a rich structure of regular and chaotic regions is typical only in a range of values of the total energy  $W$ . At the values  $W \gtrsim 40$  atoms move regularly and the respective Poincaré mapping consists of regular invariant curves only. With decreasing the energy, a series of bifurcations occurs with appearing of resonant islands of different order. When decreasing the energy even more, global chaoticity takes place. At exact resonance  $\Delta = 0$ ,

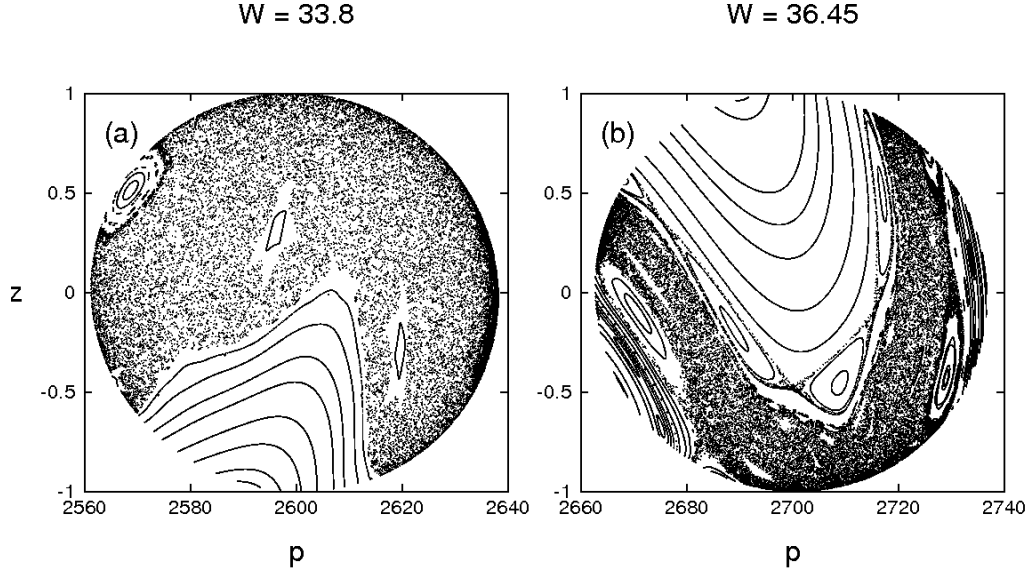


Figure 10: Poincaré mapping in the space of the momentum  $p$  and the internal energy  $z$ . (a)  $W = 33.8$ ,  $p_{\text{eff}} = 2600$ , (b)  $W = 36.45$ ,  $p_{\text{eff}} = 2700$ . The other values are the same as in Fig. 8.

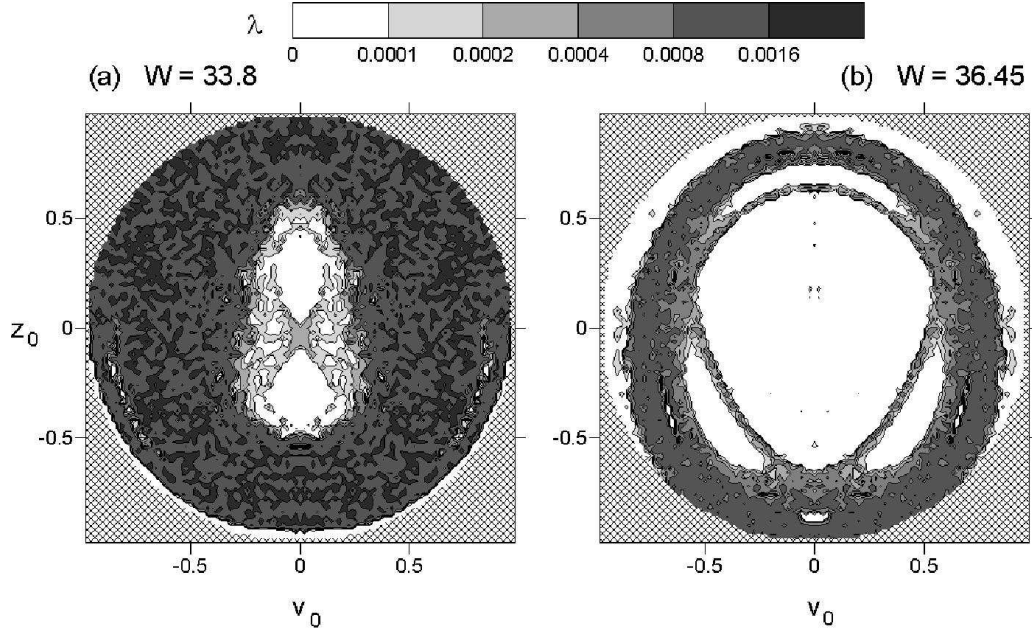


Figure 11: The maximal Lyapunov exponent vs the initial values of the Bloch variables  $v_0$  and  $z_0$  with  $u_0 > 0$ . (a)  $W = 33.8$ ,  $p_{\text{eff}} = 2600$ , (b)  $W = 36.45$ ,  $p_{\text{eff}} = 2700$ . The other values are the same as in Fig. 8.

the value  $W = u_0$  corresponds to a separatrix in mechanical variables. Out off resonance this separatrix is broken, and atoms may wander chaotically in the optical lattice with a respective irregular Poincaré mapping. At  $W \lesssim u_0 + \Delta z_0/2$  (including negative values) atoms are trapped in wells of the optical potential and oscillate there.

## 5 Conclusion

We have considered a simple model of lossless interaction between a two-level single atom and a standing-wave single-mode laser field which creates a one-dimensional optical lattice. Analytical solutions of the Hamilton-Schrödinger equations of motion have been derived and analyzed in some limiting cases of regular atomic motion. Correlations between the Rabi oscillations and the center-of-mass motion have been established and demonstrated. In the regime of chaotic wandering the atomic motion has been shown to have fractal properties. Using a special type of the Poincaré mapping of atomic trajectories in an effective three-dimensional phase space onto planes of atomic internal variables and momentum, we have found typical structures in Hamiltonian chaotic systems — chains of resonant islands of different sizes imbedded in a stochastic sea, stochastic layers, bifurcations, and so on. The phenomenon of sticking of atomic trajectories to boundaries of regular islands found in numerical experiments should have a great influence to atomic transport in optical lattices.

One of the aims of this paper was to describe analytically and numerically fundamental aspects of nonlinear dynamics of the atom-field interaction. We have done that to some extent at the cost of simplifying the model. To be more realistic we should take into account spontaneous emission events. In this case, however, the equations of motion cease to be a deterministic dynamical system because they would include random terms. Our previous results on Monte Carlo modelling Hamilton-Schrödinger equations have shown much more complicated type of atomic motion which, besides of chaotic motion, caused by the fundamental atom-field interaction, includes a purely stochastic component caused by random events of spontaneous emission. We plan to study the effects of spontaneous emission on chaotic atomic motion in the future.

## 6 Acknowledgments

This work was supported by the Russian Foundation for Basic Research (project no. 06-02-16421 “Quantum nonlinear dynamics of cold atoms in an optical lattice”), by the Program “Mathematical methods in nonlinear dynamics” of the Prezidium of the Russian Academy of Sciences (the project “Dynamical chaos and coherent structures”), and the program of the Prezidium of the Far-Eastern Division of the Russian Academy of Sciences (the projects “Non-linear quantum electrodynamics of atoms and photons” and “Dissipative dynamics of cold atoms in optical lattices”).

## References

- [1] J. Kepler, *The Harmonies of the World*, Encyclopedia Britannica, Chicago (1952).
- [2] J. C. Maxwell, *A Treatise on Electricity and Magnetism*, Dover, New York (1954).

- [3] P. N. Lebedev, *Collected Papers* [in Russian], GITTL, Moscow-Leningrad (1949).
- [4] W. Gerlach and O. Stern, *Z. Physik*, **9**, 349 (1922).
- [5] P. L. Kapitza and P. A. M. Dirac, *Proc. Comb. Philos. Soc.*, **29**, 297 (1933).
- [6] O. Frisch, *Zeit. f. Phys.*, **86**, 42 (1933).
- [7] S. Chu, *Rev. Mod. Phys.*, 685 (1998); C. Cohen-Tannoudji, *ibid*, 707 (1998); W. D. Phillips, *ibid*, 721 (1998).
- [8] S. V. Prants and L. E. Kon'kov, *JETP Letters*, **73**, 180 (2001) [*Pis'ma ZhETF*, **73**, 200 (2001)].
- [9] S. V. Prants and V. Yu. Sirotkin, *Phys. Rev. A*, **64**, art. 033412 (2001).
- [10] S. V. Prants, *JETP Letters*, **75**, 63 (2002) [*Pis'ma ZhETF*, **75**, 71 (2002)].
- [11] S. V. Prants, *JETP Letters*, **75**, 651 (2002) [*Pis'ma ZhETF*, **75**, 777 (2002)].
- [12] V. Yu. Argonov and S. V. Prants, *JETP*, **96**, 832 (2003) [*Zh. Eksp. Teor. Fiz.*, **123**, 946 (2003)].
- [13] S. V. Prants, M. Edelman, G. M. Zaslavsky, *Phys. Rev. E*, **66**, art. 046222 (2002).
- [14] A. J. Lichtenberg, M. A. Lieberman, *Regular and Stochastic Motion*, Springer, New York (1983).
- [15] V. S. Letokhov, *JETP Lett.*, **7**, 348 (1968) [*Pis'ma ZhETF*, **7**, 348 (1968)].
- [16] E. Ott, *Chaos in dynamical systems*, Cambridge University Press, Cambridge (1993).
- [17] G. M. Zaslavsky, *Hamiltonian Chaos and Fractional Dynamics*, Oxford University Press, Oxford (2005).
- [18] C. F. F. Karney, *Physica D*, **8**, 360 (1983).
- [19] B. V. Chirikov and D. L. Shepelyansky, *Physica D*, **13**, 394 (1984).
- [20] J. D. Meiss, *Rev. Mod. Phys.*, **64**, 795 (1992).
- [21] V. V. Beloshapkin and G. M. Zaslavsky, *Phys. Lett. A*, **97**, 121 (1993).